Massive Stars as Major Factories of Galactic Cosmic Rays

Felix Aharonian[1,2,3], Ruizhi Yang[2], Emma de Oña Wilhelmi[4,5]

[1]*Dublin Institute for Advanced Studies, 31 Fitzwilliam Place, Dublin 2, Ireland*
[2]*Max-Planck-Institut für Kernphysik, P.O. Box 103980, D 69029 Heidelberg, Germany*
[3]*Gran Sasso Science Institute, 7 viale Francesco Crispi, 67100 L'Aquila, Italy*
[4]*Institute of Space Sciences (ICE/CSIC), Campus UAB, Carrer de Can Magrans s/n, 08193 Barcelona, Spain*
[5]*Institut d' Estudis Espacials de Catalunya (IEEC), 08034 Barcelona, Spain*

We report a remarkable constancy of the energy and radial distribution of the CR density, $w(E,r) \propto E^{-2.3}r^{-1}$, derived around the prominent galactic clusters Westerlund 1, Westerlund 2, Cyg OB2, and, presumably, also towards three ultracompact clusters located in the Galactic Centre (GC). The $1/r$ decrement of the CR density with the distance from the star cluster is a distinct signature of continuous injection of CRs and their diffusion through ISM. The analysis of γ-ray data show that the hard energy spectra of parent protons continue up to $\sim$ 1 PeV, and the efficiency of conversion of kinetic energy of powerful stellar winds can be as high as 10 percent. This implies that the population of young massive stars can provide production of CRs at a rate of up to 10^{41} erg/s, which is sufficient to support the flux of Galactic CRs without invoking other source populations.

One of the key objectives of cosmic ray (CR) studies remains the identification of principal contributors to the *galactic component* of CRs. Most likely, hundreds or thousands of objects contribute to galactic CRs which are produced with a rate between $(0.3-1)\times10^{41}$ erg/s [1]. Therefore, the hope of identification of these objects on a source-by-source basis is unrealistic, especially given that many of these sources could not be active anymore. A more feasible approach seems to be the search for a source population, the best-studied representatives of which could (a) collectively provide the production rate of CRs in our Galaxy, and (b) explain the basic characteristics of CRs up to the so-called "knee" around 1 PeV ($1\ \mathrm{PeV} = 10^{15}\mathrm{eV}$).

The current paradigm of origin of Galactic CRs [1,2] is based on the conviction that the supernovae (SNe) explosions, in general, and their remnants (SNRs), in particular, satisfy both requirements. Over many decades, this belief has been supported by phenomenological arguments and theoretical meditations. The γ-ray observations of SNRs conducted in recent years in both high ($E \geq 0.1$ GeV) and very high (VHE; $E \geq 0.1$ TeV) energy bands did prove the effective acceleration of highly relativistic particles (electrons and/or protons/ions) in these objects [3]. However, because of the large uncertainties in gas density in the γ-ray production regions, the level of contribution of SNRs to the CR production in the Galaxy is not yet *observationally* established. More importantly, so far γ-ray observations have failed to demonstrate that SNRs can accelerate particles beyond 0.1 PeV (see the section "Methods"). As a result, a suspicion is mounting among the experts that SNRs do not operate as PeVatrons, and, thus, this source population alone cannot be responsible for the overall flux of CRs.

Meanwhile, the observations of the Galactic plane with the *Fermi* LAT and ground-based γ-ray telescopes have revealed several new classes of γ-ray sources. Potentially, some of them may provide non-negligible contribution to the observed CR flux, and thus should be considered either complementary or alternative factories of galactic CRs. In this regard, the clusters of massive young stars are of special interest. The interacting winds of massive, luminous stars have been recognised as potential CR accelerators as early as in the 1980s. The acceleration could take place on small in the vicinity of the stars [4,5] or in the so-called superbubbles, multi-parsec structures caused by the collective activity of massive OB stars around the compact stellar associations [6,7]. The acceleration on multiple shocks can rise the maximum energy of CR protons out of 10^{15}eV [8]. This makes the clusters of massive stars attractive candidates for cosmic PeVatrons.

The young star clusters contain sufficient kinetic energy, supplied by interacting stellar winds, to accelerate large amount of CRs which might be traced by γ-rays, the secondary products of CR interactions with the circumstellar and interstellar gas. The diffuse GeV and TeV γ-ray sources detected by *Fermi* LAT around compact clusters Cygnus OB2 [9], NGC 3603 [10] and Westerlund 2 [11] are naturally interpreted within this scenario. The reported hard power-law energy spectra of all three sources with similar photon indices $\Gamma \approx 2.2$ extend towards very high energies without an indication of a cutoff making them promising emitters at TeV energies as well. Detailed spectroscopic and morphological studies of moderately extended VHE γ-ray sources can be best performed with the atmospheric Cherenkov telescope arrays [12]. Diffuse TeV γ-ray structures have been indeed reported by the H.E.S.S. collaboration in the vicinity of powerful galactic clusters Westerlund 1 [13]

and Westerlund 2 [14]. as well as in 30 Dor C [15] located in the Large Magelanc Cloud.

The hard γ-ray spectra generally are interpreted as a hint for the presence of CR accelerator(s) inside or nearby the γ-ray production regions. The spectral information alone is not sufficient for identification of the accelerator. The same γ-ray spectrum can be explained within different scenarios and assumptions regarding the the object, the acceleration processes involved, the history of injection of CRs *etc*. On the other hand, the γ-ray morphology combined with the measurements of the atomic and molecular gas, can serve as a powerful tool for revealing the locations and the regime of operation of CR accelerators [16]. The method requires accurate measurement of spatial distributions of both γ-rays and the gas. It has been successfully applied, for the first time, to the diffuse TeV γ-ray emission of the Central Molecular Zone (CMZ) in the Galactic Centre (GC) [17], and, recently, also to the extended GeV γ-ray source surrounding the stellar cluster Westerlund 2 [11]. In both cases a $1/r$ type radial distributions of CRs have been revealed, pointing to the continuous operation of CR accelerators in these objects. While in the case of Westerlund 1 the association of the CR accelerator with the star cluster is straightforward, below we argue that some, or all three ultracompact star clusters, *Arches*, *Quintuplet* and *Nuclear*, are likely sites of acceleration of CRs responsible for the diffuse γ-ray emission of CMZ.

1 Results

Motivated by these results, we explored the possibility of extraction of spatial distributions of CRs in proximity of other galactic clusters embedded in diffuse γ-ray structures. The extended GeV γ-ray source around the cluster NGC 3603 [10] and the TeV γ-ray source associated with 30 Dor C [15] are too weak for derivation of statistically significant radial distributions of CRs.

On the other hand, the angular size of the diffuse GeV source associated with Westerlund 2 is too large to be detected with the current atmospheric Cherenkov telescopes.

Fortunately, in the case of Cygnus Cocoon discovered by the *Fermi* LAT collaboration as a bright extended γ-ray emitter associated with Cyg OB2 [9], and the diffuse TeV γ-ray source (HESS J1646-458) linked to Westerlund 1 [13], the photon statistics is sufficient for derivation of spectral and spatial distributions of CRs in these objects. For Cygnus Cocoon, we analysed *Fermi* LAT data using the standard LAT software package. For HESS J1646-458, we used the angular profiles published by the HESS collaboration[13]. For the distribution of molecular hydrogen, we applied the data from the CO galactic survey performed by the CfA 1.2m millimetre-wave Telescope, while for the atomic hydrogen, we used the data from the Leiden/Argentine/Bonn (LAB) Survey. The main conclusion following from the results presented in "Methods", is that the density of CR protons responsible for γ-rays, declines as r^{-1} up to $\approx$50 pc from the stellar clusters Cyg OB2 and Westerlund 1. The results are shown in Fig.1b, together with the earlier published radial distributions of CR protons in CMZ [17] and Westerlund 2 Cocoon [11]. In Fig.1b we show the differential γ-ray luminosities of these sources.

The striking similarity of both radial and energy distributions of CR protons for four different objects is a strong hint that we observe the same phenomenon. The simplest and most natural

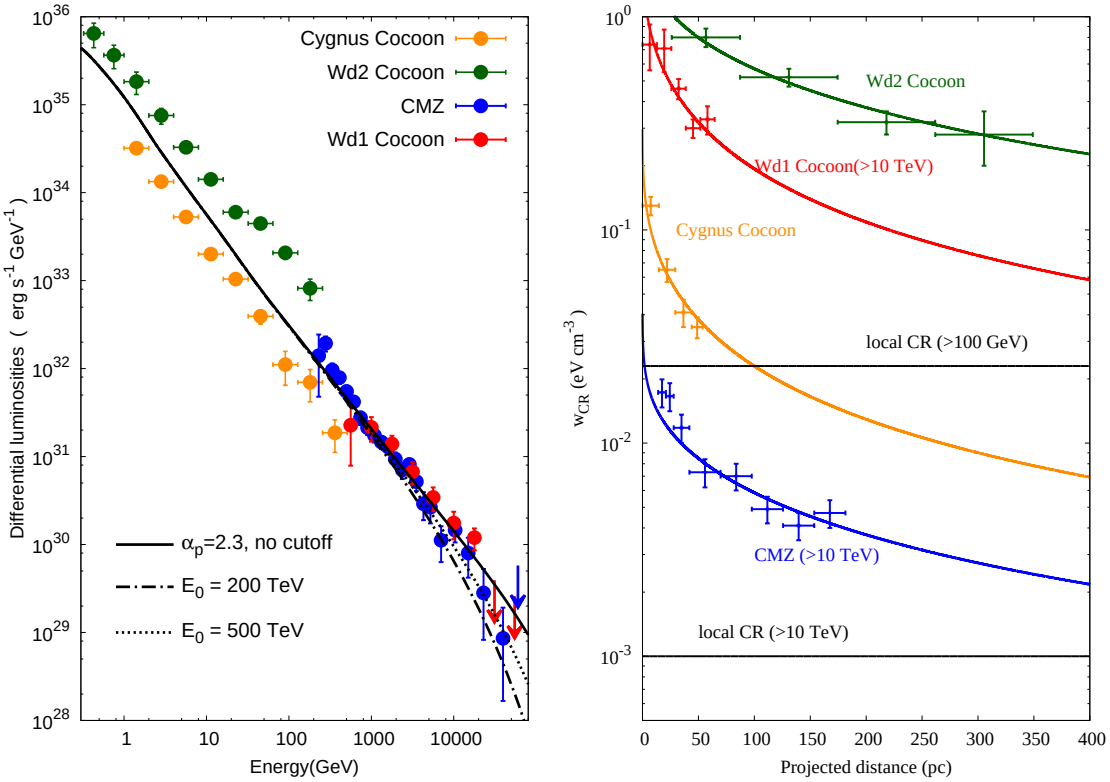

Figure 1: Gamma-ray luminosities and CR proton radial distributions in extended regions around the star clusters Cyg OB2 (Cygnus Cocoon), Westerlund 2 (Wd 2 Cocoon), and Westerlund 1 (Wd 1 Cocoon), as well as in the Central Molecular Zone (CMZ) in the Galactic Centre assuming that CMZ is powered by CRs accelerated in *Arches*, *Quintuplet* and *Nuclear* clusters. **(a)** *left panel*: The differential γ-ray luminosities, $\mathrm{d}L/\mathrm{d}E = 4\pi d^2 E f(E)$. The solid, dotted and dashed curves are calculated for the spectrum of γ-rays from pp interactions, for CR proton spectrum assuming power-law distribution with exponential cutoff, $E^{-2.3}\exp(-E/E_0)$ for $E_0 = \infty$, 0.5 PeV, and 0.2 PeV, respectively. The curves are normalised to the luminosity of CMZ at 1 TeV. **(b)** *right panel*: The CR proton radial distributions in Cyg Cocoon and Wd 2 Cocoon above 100 GeV, and in Wd 1 Cocoon and CMZ above 10 TeV. The γ-ray flux enhancement factor due to the contribution of CR nuclei was assumed $\eta = 1.5$. For comparison, the energy densities of CR protons above 100 GeV and 10 TeV based on the measurements by AMS are also shown [18].

Source	Wdr 2 Cocoon	Cyg Cocoon	CMZ	Wd 1 Cocoon
Extension (pc)	300	50	175	60
Age of cluster (Myr)[19]	1.5–2.5	3–6	2–7	4–6
L_{kin} of cluster (erg/s)	2×10^{38} [20,21]	2×10^{38} [9]	1×10^{39} [22]	1×10^{39} [23]
Dist (kpc)	5	1.4	8.5	4
$\omega_o(>100\mathrm{GeV})$ (eV/cm^3)	6	0.2	0.28	4.8

Table 1: Physical parameters of four extended γ-ray structures and the related stellar clusters

explanation of the $1/r$ dependence of CR radial distribution is that CRs have been continuously injected and diffused away through the interstellar medium (ISM). The characteristic timescales are determined by the age of the cluster, $T_0 \sim 10^6$ years; the distance scales span from ten to hundreds parsecs in ISM. This excludes SNRs as sources of CRs, and gives strong preference to massive stellar winds operating as particle accelerators. In the case of spherically symmetric diffusion, the CR density at the distance from the central source r depends on the injection rate $\dot{Q}(E)$ and the diffusion coefficient $D(E)$: $w(E,r) \propto \dot{Q}(E)/D(E)r$. On the other hand, the $1/r$ profile of CRs is independent of the absolute value of the diffusion coefficient, unless the latter varies dramatically over the scales of tens of parsecs. Generally, the diffusion coefficient is a function of energy; typically it is written in the form $D(E) = D_0(E/E_0)^\beta$. For the energy range of interest, we normalise the diffusion coefficient at $E_0 = 100$ GeV. In the Galactic Disk, D_0 is believed to be close to 10^{29} cm^2/s,

(see e.g. [24]). Inside the accelerators and in the vicinity of powerful objects, the diffusion coefficient could significantly deviate from the average interstellar value. Because of the energy-dependence of diffusion coefficient, CR spectra outside the accelerators may suffer significant modification, $\mathrm{d}N/\mathrm{d}E \propto \dot{Q}(E)/D(E) \propto E^{-(\alpha_0+\beta)}$, where α_0 is the power-law index characterising the initial (acceleration) spectrum.

The above simple relations are valid when the energy losses of CRs can be neglected. While for CR protons and nuclei this is a "safe" assumption, relativistic electrons undergo severe energy losses. However, it is quite clear that electrons cannot be responsible for the observed γ-ray images. Here we do not face the standard for SNRs question leptonic or hadronic? [3]. The leptonic (inverse Compton; IC) origin of gamma-rays is robustly excluded both at GeV and TeV energies. Firstly, the propagation of multi-TeV electrons in ISM hardly could exceed 100 pc [25]. Moreover, inside the cluster of a typical size of a few pc and total luminosity of $L_\mathrm{r} \approx 10^{40}$ erg/s, the energy density of starlight is estimated $u_\mathrm{r} \sim L/4\pi r^2 c \geq 100$ eV/cm^3. Outside the cluster, it decreases as $1/r^2$, thus, up to tens of parsecs, it dominates over the average radiation density in ISM. Therefore, in the case of IC origin of γ-rays, we would expect a sharp increase of the γ- ray intensity towards the cluster with a bright central source coinciding with the cluster. The brightness distributions of the observed γ-ray images apparently do not agree with this prediction.

The radial distribution of the CR density is convenient to present in the form

$$w(r) = w_0(r/r_0)^{-1} \,. \tag{1}$$

Below we will adopt $r_0 = 10$ pc, i.e. normalise the CR proton density w_0 outside but not far from the region occupied by the stars of the cluster. The parameter $w_0(\geq 100$ GeV) for Westerlund 2 Cocoon and Cygnus Cocoon is 6 eV/cm^3 and 0.2 eV/cm^3, respectively. At the lack of information in the GeV band, the TeV observations of Westerlund 1 Cocoon and CMZ give the energy density of protons only above 10 TeV: $w_0(\geq 10$ TeV) ≈ 1.2 eV/cm^3 and 0.07 eV/cm^3, respectively. However, under a reasonable assumption that the $E^{-2.3}$ type spectrum of relativistic protons continuous down to 100 GeV, we can calculate the energy density in these two objects above 100 GeV by multiplying $w_0(\geq 10$ TeV) by the factor of $100^{0.3} \approx 4$. The directly derived or renormalised values of the parameter $w_0(\geq 100$ GeV) are presented in Table 1.

The overall energy in CR protons responsible for detected γ-ray luminosity L_γ depends only on the average gas density in the γ-ray production region n:

$$W_{\rm p}(\geq 10E) = L_\gamma(\geq E)\, t_{\pi^0}\, \eta^{-1}\,, \tag{2}$$

where $t_{\pi^0} \simeq 1.5{\times}10^{15} n^{-1}$ s is the cooling time of protons through the channel of π^0 production and decay; the parameter η takes into account the production of γ-rays in interactions with involvement of nuclei of both CRs and ISM. Apparently, this estimate is relevant to CR protons confined in the γ-ray production region, but does not concern the more fundamental quantity, the entire energy released in accelerated particles.

For the radial distribution of CRs, given in the form of Eq.(1), the total energy of CR protons within the volume of the radius R_0 is

$$W_{\rm p} = 4\pi \int_0^{R_0} w(r) r^2\, {\rm d}r = 2\pi w_0 R_0^2 \approx 2.7\times 10^{47} (w_0/1\ {\rm eV/cm^3})({\rm R_0}/10\ {\rm pc})^2\ {\rm erg}\,. \tag{3}$$

For given w_0, the main uncertainty in this estimate is related to the upper limit of integration, R_0. If we use for R_0 the distances $R_{\rm obs}$ corresponding to the last points in Fig.1b, we obtain $W_{\rm p} \approx 1.5\times 10^{51}, 3.2\times 10^{49},\ 1.4\times 10^{48},\ 2.3\times 10^{49}$ ergs for Westerlund 2 Cocoon, Westerlund 1 Cocoon, Cygnus Cocoon, and CMZ, respectively. These estimates are less biased compared to the approach based on Eq.(2). Yet, this estimate strongly depends on the measured value of $R_{\rm obs}$ which is determined by the brightness of the γ-ray image (and, hence, depends on the gas density). The extensions of the large diffuse structure, $R_{\rm obs}$, depend also on the detector's performance, the level of the background or foreground components, *etc.* Thus, the content of CR protons within $R_{\rm obs}$ does not provide information about *all* CRs injected into ISM. The latter can be calculated by integrating Eq.(1) up to the so-called diffusion radius, $R_{\rm D}(E)$, which corresponds to the maximum distance penetrated by a particle of energy E during the operation of the accelerator T_0. In the case of negligible energy loses of propagating particles, $R_{\rm D}(E) = 2\sqrt{T_0 D(E)}$ (see e.g. [16]). The age of the individual clusters discussed here are well known and vary in a narrow range between 2 and 5 Myr. Then, for the characteristic size of the extended source filled by CRs, we have

$$R_{\rm D} \approx 1.1\times 10^3 (D_{29} T_6)^{1/2}\ \ {\rm pc}, \tag{4}$$

The diffusion coefficient cannot be very large, otherwise the demand on the total energy in CRs would exceed the available energy contained in the stellar winds, $W_{\rm CR} = f L_0 T_0 = 3\times 10^{51} f L_{38} T_6$ erg, where $L_{38} = 10^{38} L_0$ is the total luminosity of the stellar winds of the cluster in units of 10^{38} erg/s and f is the efficiency of conversation of the wind kinetic energy to CRs. Substituting $R_0 = R_{\rm D}$ into Eq.(3), we obtain

$$f \approx 1 w_0 D_{29} L_{38}^{-1} \tag{5}$$

The large resolved size (300 pc) and the large CR density in Westerlund 2 ($w_0 = 6\,\mathrm{eV/cm^3}$), combined with the well known age (2×10^6 yr) and the available energy budget in the form of kinetic energy of stellar winds (2×10^{38} erg/cm^{2}s), robustly constrain the CR acceleration efficiency in the cluster and the diffusion coefficient in its Cocoon. Indeed, from the obvious condition $R_{\rm obs} \leq R_{\rm D}$, Eq.(4) gives $D_{29} \geq 0.04$. Substituting this lower limit into Eq.(5), we obtain $f \sim 0.1$, i.e. the acceleration efficiency should be as large as 10 percent. Actually, depending on the shape of the CR spectrum below 100 GeV, the lower limit for f could be by a factor of few higher. This implies that for any reasonable acceleration efficiency, the upper and lower limits on the diffusion coefficient shrink its value to few times 10^{27} cm^2/s, significantly smaller than the diffusion coefficient in the interstellar medium.

The requirements to the parameters of other clusters are less stringent because of the smaller values of the (resolved) extensions of γ-ray sources and/or the lower CR densities. However, the reported angular extensions of γ-ray sources could not be used as unbiased measures of the real physical size of the object. For example, to measure the extension of the gamma-ray source up to a few hundred pc in TeV energies, one would need Cherenkov telescopes with adequate sensitivity over the field with angular radius more than 5 degree. Given the high γ-ray fluxes, especially at multi-TeV energies, this should be possible with the future Cherenkov Telescope Array [26].

The parameter w_0 experimentally derived fror the detected images of γ-rays, are more objective quantities. In particular the comparable values of w_0 in Westerlund 2 Cocoon and Westerlund 1 Cocoon (taking into account that the densities in these objects are derived in different energy bands) seems quite natural given the almost identical parameters of characterising these two clusters of massive stars. On the other hand, the significantly low level of the CR density in Cygnus Cocoon and CMZ, can be explained either by the low efficiency of conversion of the kinetic energy of the winds to CRs, and/or faster diffusion of relativistic particles in these objects. The case of CMZ is especially interesting, given that the total kinetic energy power in three ultracompact (Arches, Quintuplet and Nuclear) clusters is $L \simeq 10^{39}$ erg/s, i.e. exceeds by an order of magnitude the overall stellar wind power in Westerlund 1 and Westerlund 2. One can see from Eq.(5) that the acceleration efficiency could significantly, in principle, exceed 1 percent, provided that the diffusion coefficient in CMZ is much larger than in Westerlund 2 Cocoon. Although this cannot be *a priori* excluded, the alternative assumption regarding the low efficiency of CR acceleration seems a more likely option given the unusual nature of these ultracompact clusters where tens of massive OB stars are packed within the few pc linear size regions. Actually, the acceleration efficiency exceeding 10 percent, as derived for Westerlund 2, should not be typical for all star clusters. Otherwise, it would lead to overproduction of CRs, given that the overall kinetic energy power of massive stellar winds exceeds 10^{42} erg/s.

The energy spectra of CRs associated with star clusters also agree with the phenomenological concept of Galactic CRs which gives preference to very hard, E^{-2} type source spectra of CRs predicted by the DSA mechanism (see e.g. [27]). The spectra of γ-rays of *all* for diffuse sources discussed here are described by power-law energy distributions with a photon index $\Gamma \approx 2.2$. Because of the increase of the π^0-meson production cross-section with energy, the spectrum of

γ-rays appears slightly harder compared to the spectrum of parent protons [28]. In particular, over two decades in energy, $\alpha_{\rm p} \approx \Gamma + 0.1$, where $\alpha_{\rm p}$ is the power-law index of protons currently confined in the γ-ray production region. It is formed from the initial (acceleration) spectrum of protons, $\dot{Q}(E) \propto E^{-\alpha_0}$, but modified due to the energy dependent diffusion of protons, $J_{\rm p}(E,r) \propto \dot{Q}(E)/D(E)r^{-1}$. For the Kolmogorov type turbulence, $D(E) \propto E^{1/3}$, we arrive at a "classical" E^{-2} type acceleration spectrum.

The hard γ-ray spectra of Wd1 Cocoon and CMZ continue up to 20-30 TeV without an indication of a cutoff or a break (see Fig.1a). Correspondingly, the energy spectra of parent protons should not break at least until 0.5 PeV. This is an issue of great importance indicating that the massive stars can operate as PeVatrons (machines accelerating particles to energies 10^{15}eV and more). Remarkably, the potential of stellar winds (and their advantages compared to SNRs!) to accelerate protons to PeV energies, has been foreseen by Cesarsky and Montmerle as early as 1983! [5].

2 Discussion

The clusters of massive stars offer a viable solution to the long-standing problem of the origin of Galactic CRs with the ordinary (although very massive and luminous) stars as the major contributors to observed fluxes of CRs up to the *knee* around 1 PeV. Regarding the total available energetics and the efficiency of conversion of kinetic energy to nonthermal particles, the population of young stellar clusters and SNRs are an equally good choice. The same is true for the characteristic speeds of outflows (stellar winds and SNR shocks) of several thousand km/s, which is a key condition for effective realisation of the diffusive shock acceleration mechanism in the PeVatron regime. Notwithstanding, we argue that the stellar clusters have certain advantages compared to SNRs: (1) while the acceleration efficiency in stellar clusters can be as high as 10 percent, so far we do not have such a model-independent efficiency estimate for SNRs; (2) while the hard power-law spectra of γ-rays from extended regions surrounding the stellar clusters undoubtedly are of hadronic origin and continue to 10 TeV and beyond, the hadronic origin of γ-rays from SNRs is not yet established, and, in any case, the spectra of SNRs including the prominent representatives like Tyco, Cas A and SN 1006, are steep or contain cutoffs at lower energies. The clusters of massive stars are potential sources of multi-TeV neutrinos with a fair chance to be detected by the cubic-km volume neutrino detectors. In particular, Westerlund 1, which has the highest γ-ray flux at 20 TeV among all TeV γ-ray sources, seems an especially promising target for neutrino observations [29].

To conclude, we believe that the "Occam's razor" applied to two source populations would give the preference to massive-star clusters as PeVatrons substantially contributing to galactic CRs. The extension of spectrometric and morphological γ-ray measurements up to 100 TeV in the energy spectrum and up to several degrees in the angular size, from regions surrounding powerful stellar clusters would provide crucial information about the origin of CRs in general, and the physics of proton PeVatrons, in particular. Such observations with the Cherenkov Telescope Array will be available in coming years.

References

1. Drury, L. O. Origin of Cosmic Rays. *Astropart.Phys.* **39-40**,52–60 (2012). 1203.3681.

2. Blasi, P. The origin of galactic cosmic rays. A&A Rev. **21**, 70 (2013). 1311.7346.

3. Aharonian, F. A. Gamma rays from supernova remnants. *Astroparticle Physics* **43**,71–80 (2013).

4. Casse, M. & Paul, J. A. Local gamma rays and cosmic-ray acceleration by supersonic stellar winds. ApJ **237**, 236–243 (1980).

5. Cesarsky, C. J. & Montmerle, T. Gamma rays from active regions in the galaxy - The possible contribution of stellar winds. Space Sci. Rev. **36**, 173–193 (1983).

6. Bykov, A. M. & Toptygin, I. N. Interstellar turbulence and the kinetics of cosmic rays. *Akademiia Nauk SSSR Izvestiia Seriia Fizicheskaia* **46**,1659–1662 (1982).

7. Parizot, E., Marcowith, A., van der Swaluw, E., Bykov, A. M. & Tatischeff, V. Superbubbles and energetic particles in the Galaxy. I. Collective effects of particle acceleration. A&A **424**, 747–760 (2004). astro-ph/0405531.

8. Klepach, E. G., Ptuskin, V. S. & Zirakashvili, V. N. Cosmic ray acceleration by multiple spherical shocks. *Astroparticle Physics* **13**,161–172 (2000).

9. Ackermann, M. *et al.* A Cocoon of Freshly Accelerated Cosmic Rays Detected by Fermi in the Cygnus Superbubble. *Science* **334**, 1103– (2011).

10. Yang, R.-z. & Aharonian, F. Diffuse γ-ray emission near the young massive cluster NGC 3603. A&A **600**, A107 (2017). 1612.02250.

11. Yang, R.-z., de Oña Wilhelmi, E. & Aharonian, F. Diffuse gamma-ray emission in the vicinity of young star cluster Westerlund 2. *ArXiv e-prints* (2017). 1710.02803.

12. Aharonian, F., Buckley, J., Kifune, T. & Sinnis, G. High energy astrophysics with ground-based gamma ray detectors. *Reports on Progress in Physics* **71**,096901 (2008).

13. Abramowski, A. *et al.* Discovery of extended VHE γ-ray emission from the vicinity of the young massive stellar cluster Westerlund 1. A&A **537**, A114 (2012). 1111.2043.

14. Abramowski, A. *et al.* Revisiting the Westerlund 2 field with the HESS telescope array. A&A **525**, A46 (2011). 1009.3012.

15. Abramowski, A. *et al.* The exceptionally powerful TeV γ-ray emitters in the Large Magellanic Cloud. *Science* **347**, 406–412 (2015). 1501.06578.

16. Aharonian, F. A. & Atoyan, A. M. On the emissivity of πˆ0ˆ-decay gamma radiation in the vicinity of accelerators of galactic cosmic rays. A&A **309**, 917–928 (1996).

17. Abramowski, A. *et al.* Acceleration of petaelectronvolt protons in the Galactic Centre. Nature **531**, 476–479 (2016). 1603.07730.

18. Aguilar, M., Aisa, D., Alpat, B. & et al. Precision Measurement of the Proton Flux in Primary Cosmic Rays from Rigidity 1 GV to 1.8 TV with the Alpha Magnetic Spectrometer on the International Space Station. *Physical Review Letters* **114**,171103 (2015).

19. Figer, D. F. Young Massive Clusters. InBresolin, F.,Crowther, P. A. & Puls, J. (eds.) *Massive Stars as Cosmic Engines*, vol. 250 of *IAU Symposium*, 247–256 (2008). 0801.4178.

20. Rauw, G. *et al.* Early-type stars in the core of the young open cluster Westerlund 2. A&A **463**, 981–991 (2007). astro-ph/0612622.

21. Reimer, O. *et al.* VHE gamma-rays from Westerlund 2 and implications for the inferred energetics. In Hamann, W.-R., Feldmeier, A. & Oskinova, L. M. (eds.) *Clumping in Hot-Star Winds*,195 (2008). 0710.3418.

22. Muno, M. P. *et al.* Diffuse, Nonthermal X-Ray Emission from the Galactic Star Cluster Westerlund 1. ApJ **650**, 203–211 (2006). astro-ph/0606492.

23. Hußmann, B. *The Quintuplet cluster - A young massive cluster study based on proper motion membership*. Ph.D. thesis Universität Bonn ¡EMAIL¿hussmann@astro.uni-bonn.de¡/EMAIL¿ (2014).

24. Strong, A. W., Moskalenko, I. V. & Ptuskin, V. S. Cosmic-Ray Propagation and Interactions in the Galaxy. *Annual Review of Nuclear and Particle Science* **57**,285–327 (2007). astro-ph/0701517.

25. Atoyan, A. M., Aharonian, F. A. & Völk, H. J. Electrons and positrons in the galactic cosmic rays. Phys. Rev. D **52**, 3265–3275 (1995).

26. Cherenkov Telescope Array Consortium, T. *et al.* Science with the Cherenkov Telescope Array. *ArXiv e-prints* (2017). 1709.07997.

27. Malkov, M. A. & Drury, L. O. Nonlinear theory of diffusive acceleration of particles by shock waves. *Reports on Progress in Physics* **64**,429–481 (2001).

28. Kelner, S., Aharonian, F. A. & Bugayov, V. Energy spectra of gamma-rays, electrons and neutrinos produced at proton-proton interactions in the very high energy regime. *Phys.Rev.* **D74**, 034018 (2006). astro-ph/0606058.

29. Bykov, A. M., Ellison, D. C., Gladilin, P. E. & Osipov, S. M. Ultrahard spectra of PeV neutrinos from supernovae in compact star clusters. MNRAS **453**, 113–121 (2015). 1507.04018.

Methods

3 Fermi data analysis of Cygnus Cocoon

For the analysis of *Fermi* LAT data, we have selected observations towards Cygnus region for a period of more than 9 years (MET 239557417 – MET 532003684), and used the standard LAT analysis software package *v10r0p5*[1]. The $P8\_R2\_v6$ version of the post-launch instrument response functions (IRFs) was used, and both the front and back converted photons were selected.

For the region-of-interest (ROI), a $15^\circ \times 15^\circ$ square area centred on the point of $RA_{\rm J2000} = 307.17^\circ$, $DEC_{\rm J2000} = 41.17^\circ$ has been chosen. The observations with "rock angles" larger than 52° were excluded. In order to reduce the effect of the Earth albedo background, we also excluded the time intervals when the parts of the ROI were observed at zenith angles $> 90^\circ$. Also, for the spatial analysis, given the crowded nature of the region and the large systematic errors due to a poor angular resolution at low energies, we selected only photons with energies exceeding 10 GeV at which the angular resolution is significanty improved achieving to $\sim 0.1^\circ$. Note that this energy cut dramatically reduces the possible contribution of pulsars which are bright only at energies below a few GeV.

The γ-ray count map above 10 GeV in the $10^\circ \times 10^\circ$ region around Cygnus Cocoon is shown on the left panel of Fig. 1a. We performed a binned likelihood analysis by using the tool *gtlike*. The point sources listed in the 3rd Fermi source catalog (3FGL) [30] are also shown; the identified sources are shown with blue crosses, while the red crosses indicate the positions of non-identified objects in the 3FGL catalog. We also added the background models provided by the Fermi collaboration (gll_iem_v06.fits and _P8R2_SOURCE_V6_v06.txt for the galactic and the isotropic diffuse components, respectively[2]). In the analysis, the normalisations and the spectral indices of sources inside the FOV were left free. We used the 2-D gaussian template provided by Fermi Collaboration to model the extended emission from the Cygnus Cocoon. We varied the position and the radius of the Cygnus Cocoon template but did not find a significant improvement. Therefore, for derivation of the energy spectrum we use the 2D gaussian template provided by the *Fermi* LAT Collaboration. In the ROI two TeV sources are also detected [31], Gamma Cygni and TeV J2032+415. We note that both of them are already identified in the 3FGL catalog and included in this analysis. The position of both sources are shown in the right panel of Fig. 1.

To derive the spectrum we divided the energy interval $0.5\ {\rm GeV} - 500\ {\rm GeV}$ into 10 logarithmically spaced bands and applied the tools *gtlike* to each of these bands. The derived SEDs Cygnus Cocoon are shown in Fig. 2. In general, the spectral points are consistent with the results reported in [9]. However, the larger photon statistics and the new data reduction tools allow significant extension of the spectrum, up to 500 GeV. The spectrum above 1 GeV can be well fitted with a power law with a photon index of 2.2 ± 0.1 and the integrated flux of $1.0 \pm 0.1\ \times 10^{-7} {\rm ph\ cm^{-2}\ s^{-1}}$. The detected spectrum extends to 500 GeV without an indication of a cut-off or a break. Correspond-

[1] http://fermi.gsfc.nasa.gov/ssc

[2] available at http://fermi.gsfc.nasa.gov/ssc/data/access/lat/BackgroundModels.html

ingly, the parent protons should have a power-law spectrum with a slightly larger (≈ 0.1 spectral index up to $\approx 20 \times 0.5$ TeV $= 10$ TeV) [28]. This is demonstrated in Fig. 2 where the energy spectra of γ-rays calculated for the proton spectrum with the power-low index 2.3 and exponential cutoffs at different energies are shown.

We should note that multi-TeV γ-rays have been claimed from Cygnus Cocoon by the MILAGRO [31] and ARGO [32] collaborations. The comparison of spectral points from different experiments requires a special and non trivial treatment given the statistical and systematic uncertainties concerning the energy measurements, as well as the different extensions of the regions from which the γ-rays have been detected. Nevertheless, for the sensitivities of these detectors, the reported fluxes hardly could appear below the extrapolation of the *Fermi LAT* spectrum of Cygnus Cocoon.

.

4 Gas distribution

We use the data from the CO galactic survey of [33] performed with the CfA 1.2m millimetre-wave Telescope as well as the HI data from the Leiden/Argentine/Bonn (LAB) Survey. For the CO data, we use the standard assumption of a linear relationship between the velocity-integrated CO intensity, $W_{\rm CO}$, and the column density of molecular hydrogen, N(H_2), adopting for the conversion factor $X_{\rm CO} = 2.0 \times 10^{20}$ cm^2(K km s^{-1})$^{-1}$ [34]. For the HI data we use the equation

$$N_{HI}(v, T_s) = -log\left(1 - \frac{T_B}{T_s - T_{bg}}\right) T_s C_i \Delta v \ , \tag{6}$$

where $T_{bg} \approx 2.66$ K is the brightness temperature of the cosmic microwave background radiation at 21cm, and $C_i = 1.83 \times 10^{18}$ cm^2. For $T_B > T_s - 5$ K, we truncate T_B to $T_s - 5$ K; T_s is chosen to be 150 K.

The Cygnus region is located inside the Local Arm, although the Perseus and the outer arms also contribute to the total gas content in the line of sight. To select the gas content related to Cygnus Cocoon itself, we separate, following [35], two regions contributing to the total gas. In the $\rm H_I$ and CO maps, we assign the gas with $V_{\rm LSR} < -20$ km/s to be Local arm and those with $V_{\rm LSR} > -20$ km/s to be outer arms. The gas content related to the local arms are regarded to be connected with extended γ-ray emission in Cygnus Cocoon. The gas mass is derived in the region defined by the γ-ray 2D template.

The Cygnus region harbours huge amount of $\rm H_{II}$ gas. To determine the $\rm H_{II}$ column density, we use the Planck free-free map [36]. First, we convert the emission measure (EM) in the Planck map into the free-free intensity by using the conversion factor in Table 1 of [38]. Then, we used Eq. (5) of [37] to calculate the $\rm H_{II}$ column density from the intensity of free-free emission. One should note that the derived $\rm H_{II}$ column density is inversely proportional to the electron density n_e which is chosen here to be 2 cm^{-3} [37] as a fiducial value. Summing all gas phase the total mass amounts to $2 \times 10^6 M_\odot$. For the radius of the Cygnus Cocoon of 70 pc, the average gas density is estimated

between 10 to 20 cm^{-3}, given the approximately 50% uncertainty in the mass estimate. We also note that the $\mathrm{H_{II}}$ component only contributes about 20% of the total gas content, the exclusion of this component does not alter the results of the next section.

For Wd1 Cocoon we also perform a kinetic separation, the velocity range $-60\ \mathrm{km/s} < \mathrm{V_{LSR}} < -50\ \mathrm{km/s}$[13] for both $\mathrm{H_I}$ and CO maps are chosen in this analysis. The gas content is shown in Fig.4. The total gas mass in the TeV γ-ray emission region (about 1° around Westerlund 1) is about $3 \times 10^5 M_\odot$.

5 Radial distribution of Cosmic rays

The brightness distribution of γ-rays is shaped by the product of spatial distributions of CRs and the gas density. In ISM, the dense gas complexes are distributed rather chaotically. Therefore, the probability of detection of an "ordered" γ-ray image is small. In particular, the $1/r$ type smooth radial distributions of CRs originating from the young star clusters Cyg OB2 and Westerlund 2, are derived from quite irregular γ-ray images. The position of the star cluster Cyg OB2 is significantly shifted from the centre of the surrounding γ-ray image (see Fig.1). Moreover, in the case of of Wd2, the star cluster is located at the periphery of the γ-ray image (see Fig.4 of [11]).

The comparison of the spatial distributions of the γ-ray brightness and the gas density derived in the previous sections does not show linear correlation which one would expect in the case of homogeneously distributed parent CRs.

To investigated the CR distribution, we produce the radial profile of the the γ-ray emissivity, which is proportional to the CR density.

Cygnus Cocoon As the reference point we take the position of the stellar cluster Cygnus OB2. As noted above, Cygnus OB2 is not symmetrically located inside the γ-ray image of the Cygnus Cocoon. Its choice as the reference point is motivated by the hypothesis that the massive OB stars of this cluster are the main producers of CRs responsible for the γ-ray emission.

The γ-ray flux is derived above 10 GeV, using the standard likelihood analysis, for five rings centred on Cygnus OB2 within the following angular radii: [0:0.4]°, [0.4:0.8]°, [0.8:1.4]° [1.4:1.8]° and [1.8:2.2]°. We note that the presence of the bright γ-ray pulsar LAT PSR J2023+4127 close to Cygnus OB2 may introduce additional contamination. To minimise the impact of this pulsar, we performed the so-called pulsar gating analysis. Namely, we produced the phase-folded light curve of LAT PSR J2023+4127 using the ephemeris corresponding to the time interval from MJD 54658 to 56611[3]. To obtain the light curve, we adopted a 1° aperture without applying any background subtraction above 1 GeV. The resulted light curve is shown in Fig. 5. It shows two peaks located at the phases 0.5 and 0.95, respectively. Therefore, in order to remove the pulsed emission, the γ-ray data have been selected only for the phase intervals [0.1,0.4] and [0.6,0.9]. In this way, we

[3] see https://confluence.slac.stanford.edu/display/GLAMCOG/LAT+Gamma-ray+Pulsar+Timing+Models

dramatically reduce the impact of the bright γ-ray pulsar, albeit at the expense of reduction of the γ-ray photon statistics by 40%,

The total gas column density is contributed by the molecular, neutral atomic and ionised hydrogen components as discussed in previous section. The comparison of spatial distributions of the γ-ray intensity and the overall gas column density gives the radial profile of γ-ray emissivity, and consequently provides direct information about the profile of the CR density.

The derived radial profile of the γ-ray emissivity is shown in Fig. 6 together with two curves corresponding to (i) the the homogeneous distribution of CRs which is formed in the case of an impulsive injection event, and (ii) $1/r$ type distribution of CRs, whoch is expected in the case of continuous injection of CRs into ISM. The latter distribution is favoured, with a χ^2/ndf of 0.99 versus a χ^2/ndf of 31.0, compared to the case of homogeneous distribution of CRs.

We note that the TeV source TeV J2032+415 [39] coincides in position with the pulsar LAT PSR J2023+4127 and may contaminate the most inner bin. This source has been recently identified as a variable gamma-ray source, with a flux level (above 200 GeV) increased by a factor of 2 in the recent flare event [39]. However, even without the first bin the $1/r$ type distribution of CRs are strongly favored, the χ^2/ndf is 0.8 campared with a χ^2/ndf of 15.6 in the homogeneous CR distribution case.

Wd1 Cocoon We use the H.E.S.S published results for the radial profile of the VHE γ-ray excess [13]. Due to the limited angular resolution of the gas maps we rebinned the HESS radial profile to a binsize of 0.2°. To minimize the contamination from the nearby TeV source HESS J1640-465/J1641-463 we omit all points beyond 1.0°. The determination of gas mass is described in last section. The results of the radial distribution of γ-ray emissivities (per H-atom) are shown in the right panel of Fig.6.

Wd2 Cocoon and Central molecular zone (CMZ) The γ-ray observations towards Wd2 Cocoon and CMZ, as well as the corresponding gas distribution have been investigated in detail in the former works [17,40]. In this work we use the radial profile in these references.

CR density To derive the CR density, we used the following formular,

$$w_{\rm CR}(\geq 10E_\gamma) = \frac{W_p(\geq 10E_\gamma)}{V} = 1.8\times10^{-2}\left(\frac{\eta}{1.5}\right)^{-1}\left(\frac{L_\gamma(\geq E_\gamma)}{10^{34}{\rm erg/s}}\right)\left(\frac{M}{10^6 M_\odot}\right)^{-1}{\rm eV/cm^3}\,, \tag{7}$$

where M is the mass of the relevant region, η accounts for the presence of nuclei heavier than hydrogen in both cosmic rays and interstellar matter. η depends on the chemical composition of CRs and the ambient gas, and typically varied between $1.5 \sim 1.8$[41–43]. The γ-ray luminosity, mass estimates and resulted CR densities for all regions for Cygnus Cocoon, Wd1 Cocoon and Wd2 Cocoon are presented in Extended Data Table 1, 2 and 3. The γ-ray flux and gas mass for Wd2 Cocoon are derived in our previous work [40].

6 Supernova Remnants: the main contributors to Galactic CR?

SNRs are widely believed to be the main suppliers of Galactic CRs. This conviction is based on two sound arguments: (1) the availability of sufficient energy in the form of supernova explosions to support the required CR production rate in the Galaxy, and (2) adequate conditions in young SNRs for acceleration of relativistic parties through the mechanism of Diffusive Shock Acceleration (DSA). Yet, despite the extensive experimental and theoretical studies of CRs over the last several decades, the SNR paradigm of the origin of galactic CRs should be still confirmed.

The direct measurements of CRs are important, but they cannot address the principal question regarding the localisation and identification of particle accelerators. Therefore, the ultimate solution to this long-standing problem can be found only by astronomical means. The acceleration of CRs in SNRs and their subsequent interactions with the ambient matter make these objects potentially detectable sources of γ-rays and neutrinos [44].Indeed, over the last 20 years, many young and mid-age SNRs have been detected in GeV and TeV bands. In Fig. 8 we show the spectral measurements (in the form of differential luminosities) of several prominent representatives of young SNRs at energies above 100 GeV [45–47,47–52]. Most of them show a shell-like morphology supporting the general predictions of DSA and, thus, establishing the SNR shocks as effective particle accelerators.

The very fact of detection of VHE γ-rays does not yet prove the dominant role of SNRs in the production of galactic CRs. VHE γ-rays from young SNRs demonstrate the effective acceleration of particles to energies to 100 TeV, but it is not yet clear that the detected γ-rays are of hadronic origin. In SNRs, in addition to the γ-ray production in interactions of CR protons and nuclei with the surrounding gas, an equally important process is the Inverse Compton (IC) scattering of ultra-relativistic electrons on the 2.7K CMB photons. For this reason, the origin of γ-radiation detected from *all* SNRs is under intense debates. The interpretations within the leptonic and hadronic scenarios have 'contras' and 'pros' . Within the uncertainties of the principal parameters, both models can satisfactorily fit the broad-band γ-ray spectra [3].

'Leptonic or hadronic?' It is one of the key issues of current interpretations of γ-ray observations of SNRs. But it still does not address a more fundamental question whether SNRs are the major contributors to the Galactic Cosmic Rays? Actually, there are two questions to be addressed: (i) whether SNRs can produce cosmic rays with overall energy close to 10^{50}erg? (ii) if yes, whether they can be responsible for the locally observed CR flux up to the "knee" around 1 PeV?

The positive answer to the hadronic origin of γ-radiation would not imply a positive answer to the first question as well. Although the total energy budget in CRs $W_{\rm p}$ derived from γ-ray data in some SNRs is close to 10^{50} erg, in some others it is estimated significantly lower. One should notice that the estimates of $W_{\rm p}$ depends on the ambient gas density ($\propto 1/n$) and, therefore, contain an order of magnitude uncertainties. Concerning the second question, the term "PeVatron" implies an object accelerating protons with a hard (E^{-2} type) energy spectrum without a break up to $E \sim 1$ PeV. The spectrum of secondary γ-rays almost mimics the spectrum of the parent

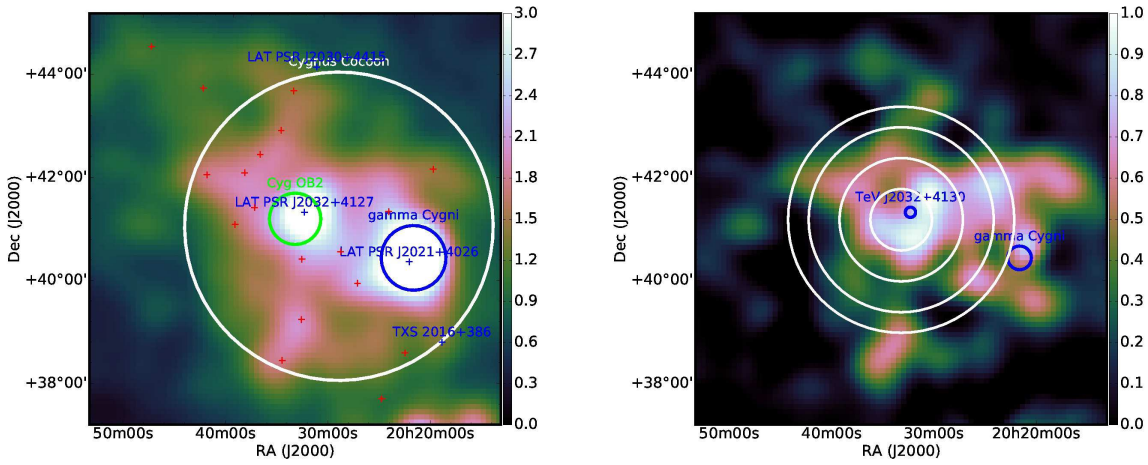

Extended Data Figure 1: The count (left panel) and residual (right panel) maps of γ-rays around the at energies above 10 GeV. A $10^\circ \times 10^\circ$ region around Cygnus Cocoon is shown. The positions of the 3FGL catalog sources are marked with blue and red crosses for the identified and unassociated *Fermi* LAT sources, respectively. Also shown is the position of the extended source Gamma Cygni (blue circle) and the position of young star association Cygnus OB2 (green circle). The residual map is obtained after subtracting all identified catalog sources as well as the diffuse backgrounds. The white circles on the residual map represent the regions used for the extraction of the radial distribution of γ-ray emissivities. The blue circles show the position and extension of two TeV sources Gamma Cygni and TeV J2032+415.

protons but is shifted towards low energies by a factor of 20-30. Thus, a detection of γ-rays with a hard-power-law energy spectrum extending several tens of TeV would imply an unambiguous detection of a PeVatron. So far, the observations of young SNRs did not reveal such hard multi-TeV energy spectra. Only a few SNRs have been detected above 10 TeV, but in all cases we see steep spectra, typically with a slope between 2.5 and 3 (see Fig. 8). This can be interpreted either large power-law indices or *early* cutoffs in the proton spectra (typically less than tens of TeV) implying that the spectra of parent protons do not extend much beyond 100 TeV. This, to a certain extent, unexpected result is a hint that either the young SNRs do not accelerate CR protons to PeV energies or the production of PeV protons takes place in objects belong a sub-class of SNRs which so far have not been detected in γ-rays. The first option would imply the inability of SNRs to play the major role in the production of galactic CRs. The second option leaves a room for "accommodation" of SNRs in the scheme of galactic CRs. But it means that only a small fraction of SNRs contribute to CRs, at least at highest energies. Consequently, one should assume that the efficiency of conversion of energy in these objects should significantly exceed the "nominal" 10 percent value.

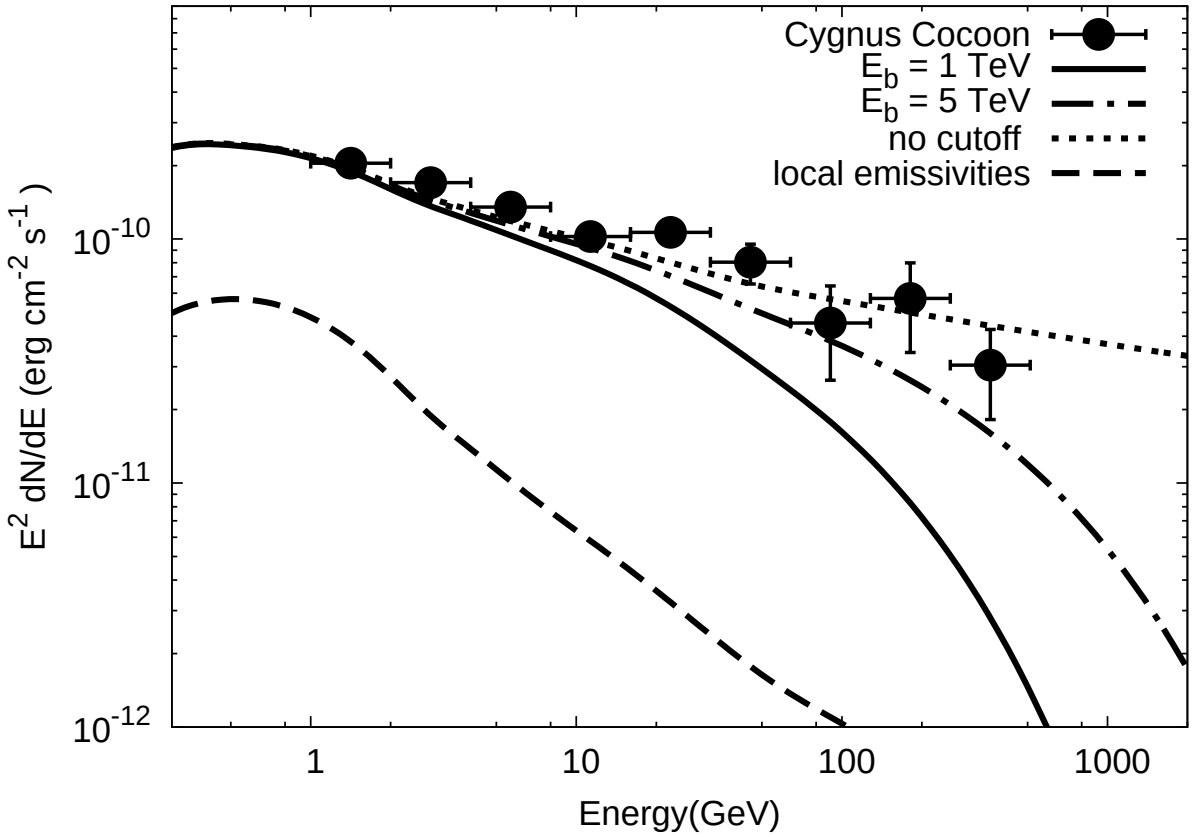

Extended Data Figure 2: The spectral energy distribution of γ-rays from Cygnus Cocoon. The theoretical curves represent the spectra of γ-rays from interactions of protons with the ambient medium, calculated for the energy distributions of protons with fixed spectral index ($\alpha_p = 2.3$) but different exponential cutoffs at energies 5 TeV, 10 TeV and 20 TeV. The dashed curve represents the predicted γ-ray emission in the H_{II} region assuming that the CR flux is identical to the flux and composition of local CRs as measured by AMS-02 [18]. The H_{II} density is derived by using Eq. (5) of [37] and the free-free radiation intensity from [36].

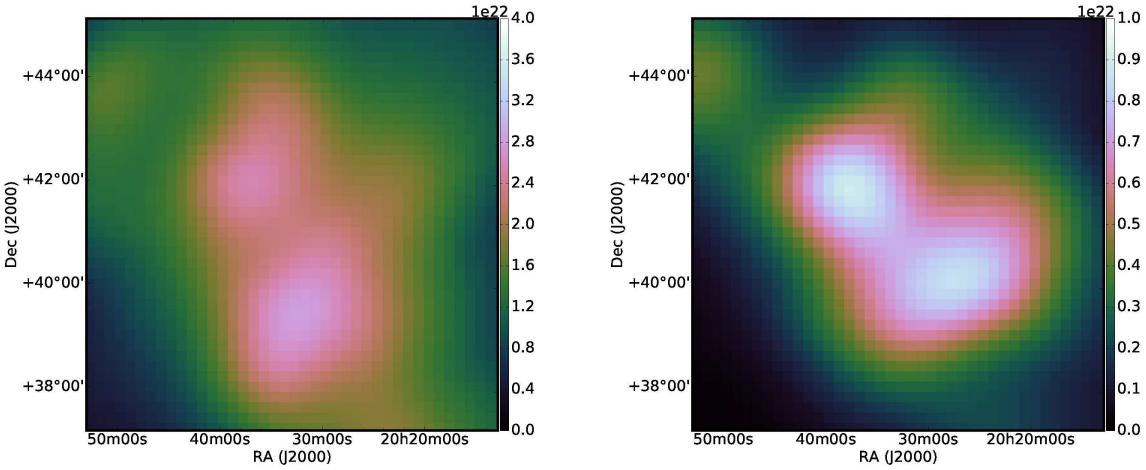

.

Extended Data Figure 3: *Left panel*: the molecular and neutral atomic hydrogen column density in the Local Arm towards Cygnus Cocoon. *Right panel*. The ionised hydrogen density derived assuming for the electron density $n_e = 2\ \mathrm{cm}^{-3}$

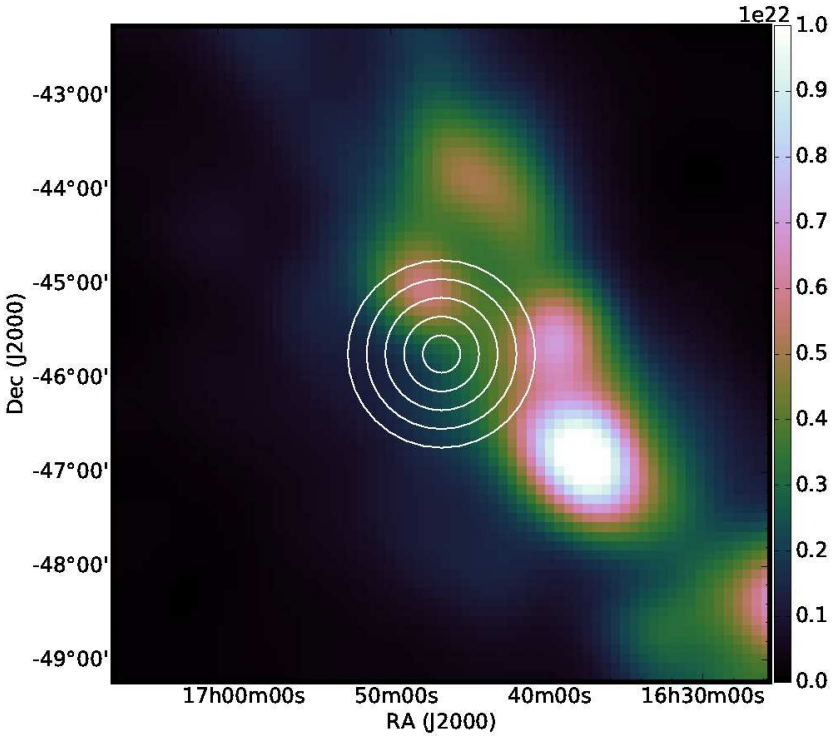

Extended Data Figure 4: The molecular and neutral atomic hydrogen column density in the vicinity of Westerlund 1. The velocity range $-60\ \mathrm{km/s} < \mathrm{V_{LSR}} < -50\ \mathrm{km/s}$ are integrated to derive the gas distribution. The green rings label the region to subtract the radial distribution of CRs.

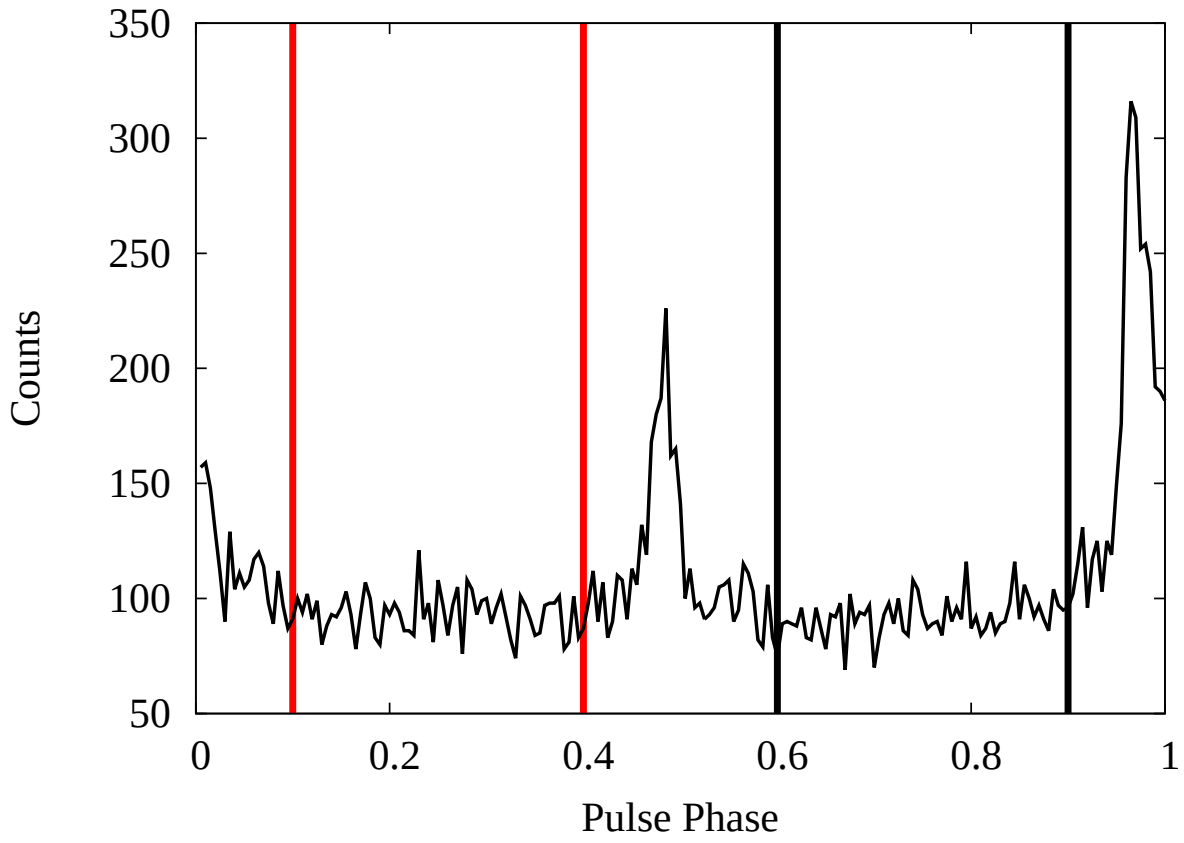

Extended Data Figure 5: Phase-folded light curve of the pulsar LAT PSR J2032+4127. The γ-ray data have been selected, for the further analysis, only for the intervals between two black and two read vertical lines.

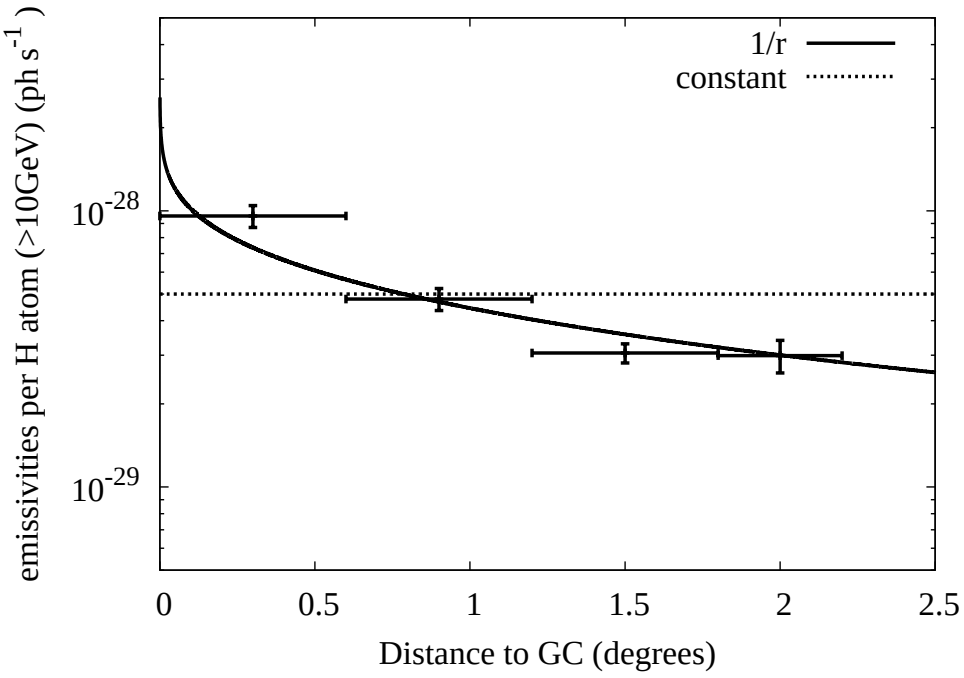

Extended Data Figure 6: The profile of γ-ray emissivities (per H-atom) above 10 GeV with respect to the location of Cygnus OB2. For comparison, we show $1/r$ (solid curve), and constant (dotted curve) profiles, which are expected in the cases of continuous and impulsive injections, respectively. The radial distributions are shown for all three (atomic, molecular and ionised) components of gas involved in the γ-ray production.

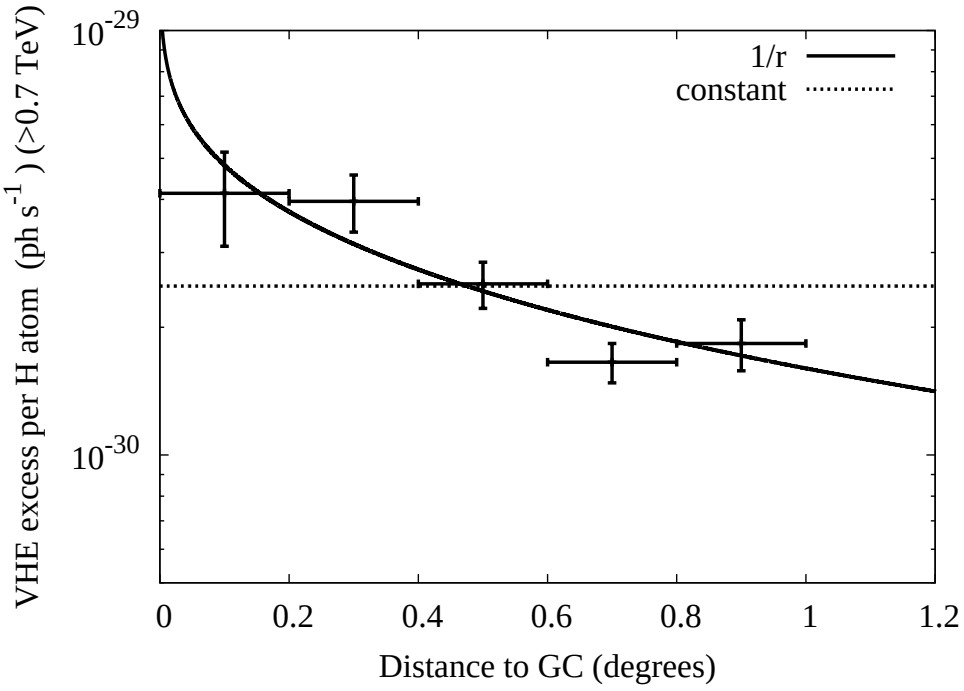

Extended Data Figure 7: The VHE excess per H-atom in the vicinity of Westerlund 1. The curves are the same as those in figure6.

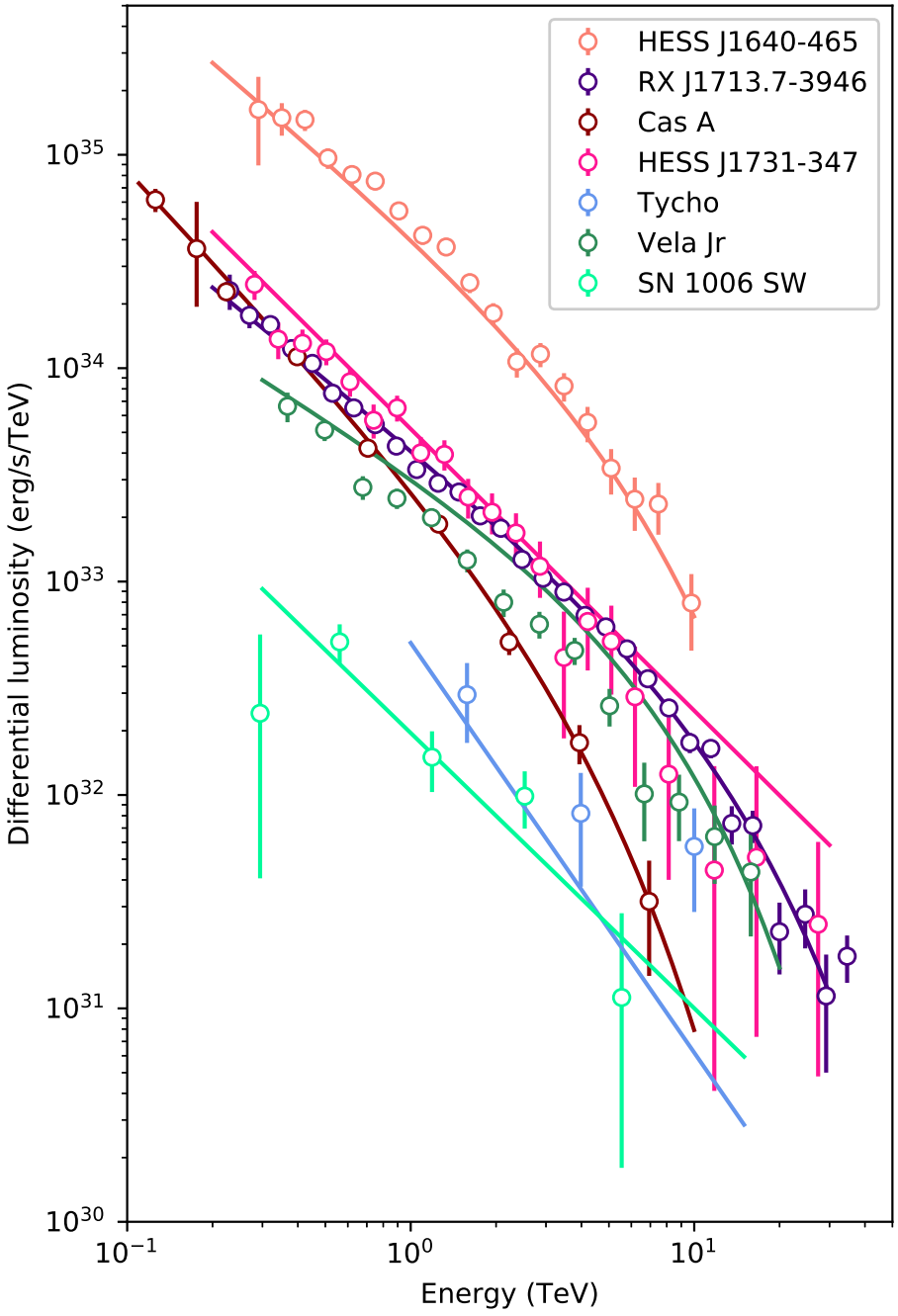

Extended Data Figure 8: Differential spectrum of several TeV-bright SNRs

Region	L_γ (>10 GeV) (10^{34}erg/s)	mass (10^5 $M_\odot$)	$w_{\rm CR}$ (> 100 GeV)(eV/cm^3)
0 pc < r < 15 pc	0.60 ± 0.06	0.8	0.13 ± 0.013
15 pc < r < 29 pc	0.87 ± 0.09	2.4	0.065 ± 0.007
29 pc < r < 44 pc	0.91 ± 0.13	4.0	0.041 ± 0.006
44 pc < r < 54 pc	0.64 ± 0.07	3.3	0.035 ± 0.004

Extended Data Table 2: γ-ray luminosities, gas masses and CR densities in different regions of the Cygnus Cocoon.

Region	L_γ (>10 GeV) (10^{34}erg/s)	mass (10^5 $M_\odot$)	$w_{\rm CR}$(> 100 GeV)(eV/cm^3)
26 pc < r < 87 pc	9.64 ± 1.60	2.2	0.80 ± 0.13
87 pc < r < 174 pc	20.4 ± 2.08	7.0	0.52 ± 0.05
174 pc < r < 260 pc	17.0 ± 1.90	9.6	0.32 ± 0.03
260 pc < r < 350 pc	14.2 ± 4.2	9.0	0.28 ± 0.08

Extended Data Table 3: γ-ray luminosities, gas masses and CR densities in different regions of the Wd2 Cocoon

Region	L_γ(>1 TeV) (10^{34}erg/s)	mass (10^5 $M_\odot$)	$w_{\rm CR}$(> 10 TeV)(eV/cm^3)
0 pc < r < 13 pc	0.41 ± 0.10	0.1	0.73 ± 0.18
13 pc < r < 26 pc	1.18 ± 0.27	0.3	0.71 ± 0.16
26 pc < r < 39 pc	1.87 ± 0.20	0.73	0.46 ± 0.05
39 pc < r < 52 pc	2.01 ± 0.27	1.20	0.30 ± 0.04
52 pc < r < 65 pc	1.92 ± 0.23	1.03	0.33 ± 0.04

Extended Data Table 4: γ-ray luminosities, gas masses and CR densities in different regions of the Wd1 Cocoon

References

30. The Fermi-LAT Collaboration. Fermi Large Area Telescope Third Source Catalog. *ArXiv e-prints* (2015). 1501.02003.

31. Abdo, A. A. *et al.* Spectrum and Morphology of the Two Brightest Milagro Sources in the Cygnus Region: MGRO J2019+37 and MGRO J2031+41. ApJ **753**, 159 (2012). 1202.0846.

32. Bartoli, B. *et al.* Identification of the TeV Gamma-Ray Source ARGO J2031+4157 with the Cygnus Cocoon. ApJ **790**, 152 (2014). 1406.6436.

33. Dame, T. M., Hartmann, D. & Thaddeus, P. The Milky Way in Molecular Clouds: A New Complete CO Survey. ApJ **547**, 792–813 (2001). arXiv:astro-ph/0009217.

34. Bolatto, A. D., Wolfire, M. & Leroy, A. K. The CO-to-H_2 Conversion Factor. ARA&A **51**, 207–268 (2013). 1301.3498.

35. Ackermann, M. *et al.* The cosmic-ray and gas content of the Cygnus region as measured in gamma rays by the Fermi Large Area Telescope. *Astron.Astrophys.* **538**,A71 (2012). 1110.6123.

36. Planck Collaboration *et al.* Planck 2015 results. X. Diffuse component separation: Foreground maps. A&A **594**, A10 (2016). 1502.01588.

37. Sodroski, T. J. *et al.* A Three-dimensional Decomposition of the Infrared Emission from Dust in the Milky Way. ApJ **480**, 173–187 (1997).

38. Finkbeiner, D. P. A Full-Sky Hα Template for Microwave Foreground Prediction. ApJS **146**, 407–415 (2003). astro-ph/0301558.

39. Mirzoyan, R. & Mukherjee, R. TeV gamma-ray emission from PSR J2032+4127/ MT91 213 at periastron. *The Astronomer's Telegram* **10971** (2017).

40. Yang, R.-z., de Oña Wilhelmi, E. & Aharonian, F. Diffuse gamma-ray emission in the vicinity of young star cluster Westerlund 2. *ArXiv e-prints* (2017). 1710.02803.

41. Dermer, C. D. Secondary production of neutral pi-mesons and the diffuse galactic gamma radiation. A&A **157**, 223–229 (1986).

42. Mori, M. Nuclear enhancement factor in calculation of galactic diffuse gamma-rays: A new estimate with dpmjet-3. *Astroparticle Physics* **31**,341 – 343 (2009).

43. Kafexhiu, E., Aharonian, F., Taylor, A. M. & Vila, G. S. Parametrization of gamma-ray production cross-sections for pp interactions in a broad proton energy range from the kinematic threshold to PeV energies. *ArXiv e-prints* (2014). 1406.7369.

44. Drury, L. O., Aharonian, F. A. & Voelk, H. J. The gamma-ray visibility of supernova remnants. A test of cosmic ray origin. A&A **287**, 959–971 (1994). astro-ph/9305037.

45. Abramowski, A. *et al.* HESS J1640-465 - an exceptionally luminous TeV γ-ray supernova remnant. MNRAS **439**, 2828–2836 (2014). 1401.4388.

46. H.E.S.S. Collaboration *et al.* A new SNR with TeV shell-type morphology: HESS J1731-347. A&A **531**, A81 (2011). 1105.3206.

47. Aharonian, F. *et al.* Discovery of Gamma-Ray Emission From the Shell-Type Supernova Remnant RCW 86 With Hess. ApJ **692**, 1500–1505 (2009). 0810.2689.

48. Aharonian, F. *et al.* H.E.S.S. Observations of the Supernova Remnant RX J0852.0-4622: Shell-Type Morphology and Spectrum of a Widely Extended Very High Energy Gamma-Ray Source. ApJ **661**, 236–249 (2007). astro-ph/0612495.

49. Aharonian, F. *et al.* Primary particle acceleration above 100 TeV in the shell-type supernova remnant ¡ASTROBJ¿RX J1713.7-3946¡/ASTROBJ¿ with deep HESS observations. A&A **464**, 235–243 (2007). astro-ph/0611813.

50. Aharonian, F. *et al.* A detailed spectral and morphological study of the gamma-ray supernova remnant ¡ASTROBJ¿RX J1713.7-3946¡/ASTROBJ¿ with HESS. A&A **449**, 223–242 (2006). astro-ph/0511678.

51. Archambault, S. *et al.* Gamma-Ray Observations of Tycho's Supernova Remnant with VERITAS and Fermi. ApJ **836**, 23 (2017). 1701.06740.

52. Ahnen, M. L. *et al.* A cut-off in the TeV gamma-ray spectrum of the SNR Cassiopeia A. MNRAS **472**, 2956–2962 (2017). 1707.01583.